

Regulation of firing frequency in a computational model of a midbrain dopaminergic neuron

Anna Y. Kuznetsova · Marco A. Huertas ·
Alexey S. Kuznetsov · Carlos A. Paladini ·
Carmen C. Canavier

Received: 10 August 2009 / Revised: 15 January 2010 / Accepted: 1 February 2010 / Published online: 10 March 2010
© Springer Science+Business Media, LLC 2010

Abstract Dopaminergic (DA) neurons of the mammalian midbrain exhibit unusually low firing frequencies *in vitro*. Furthermore, injection of depolarizing current induces depolarization block before high frequencies are achieved. The maximum steady and transient rates are about 10 and 20 Hz, respectively, despite the ability of these neurons to generate bursts at higher frequencies *in vivo*. We use a three-compartment model calibrated to reproduce DA neuron responses to several pharmacological manipulations to uncover mechanisms of frequency limitation. The model exhibits a slow oscillatory potential (SOP) dependent on the interplay between the L-type Ca^{2+} current and the small conductance K^+ (SK) current that is unmasked by fast Na^+ current block. Contrary to previous theoretical work, the SOP does not pace the steady spiking frequency in our model. The main currents that determine the spontaneous firing frequency are the subthreshold L-type Ca^{2+} and the

A-type K^+ currents. The model identifies the channel densities for the fast Na^+ and the delayed rectifier K^+ currents as critical parameters limiting the maximal steady frequency evoked by a depolarizing pulse. We hypothesize that the low maximal steady frequencies result from a low safety factor for action potential generation. In the model, the rate of Ca^{2+} accumulation in the distal dendrites controls the transient initial frequency in response to a depolarizing pulse. Similar results are obtained when the same model parameters are used in a multi-compartmental model with a realistic reconstructed morphology, indicating that the salient contributions of the dendritic architecture have been captured by the simpler model.

Keywords Multicompartmental model · Pacemaking · Depolarization block

Action Editor: Charles Wilson

A. Y. Kuznetsova · C. A. Paladini
Department of Biology and Neurosciences Institute,
University of Texas at San Antonio,
One UTSA Circle,
San Antonio, TX 78249, USA

A. Y. Kuznetsova · M. A. Huertas · C. C. Canavier (✉)
Neuroscience Center of Excellence and
Department of Ophthalmology,
Louisiana State University Health Sciences Center,
2020 Gravier St., Suite D,
New Orleans, LA 70112, USA
e-mail: ccanav@lsuhsc.edu

A. Y. Kuznetsova · A. S. Kuznetsov
Department of Mathematical Sciences and Center for Biosciences,
Indiana University and Purdue University at Indianapolis,
402 N. Blackford St, LD270,
Indianapolis, IN 46202, USA

1 Introduction

Dopaminergic signaling is important in attention, movement and motivation (Carlson 1999), and is hypothesized to play a prominent role in addictive behavior (Wise 2004) and other psychiatric (Strange 2001) and neurological disorders (Bernheimer et al. 1973). The dopaminergic (DA) neurons in the ventral tegmental area (VTA) and substantia nigra pars compacta (SNc) have a low irregular basal firing frequency in the 1–8 Hz range *in vivo* that can increase dramatically (>20 Hz) (Grace and Bunney Grace and Bunney 1984a, b; Hyland et al., 2002) in response to an unpredicted reward or a cue predicting reward; this phasic signal, or burst, is hypothesized to reinforce actions that preceded the reward (Schultz 2002). This correlation between events at the cellular and behavioral levels motivates this study.

DA neurons *in vitro* fire in a regular, low-frequency (1–8 Hz) single spiking pattern. This firing frequency has been assumed to be driven by a subthreshold oscillation (Kang and Kitai 1993a; Nedergaard et al. 1993; Ping and Shepard 1996; Yung et al 1991) called a slow oscillatory potential (SOP). Membrane currents responsible for this SOP are an L-type calcium current that drives the depolarizing phase of the oscillation and contributes to the accumulation of intracellular calcium (Chan et al. 2007), whereas an SK-type calcium-dependent potassium current produces the repolarizing phase of the oscillation (Nedergaard et al. 1993; Surmeier et al. 2005). Previous modeling approaches have shown that these currents can support pacemaking when they are restricted to the soma (Amini et al. 1999; Komendantov et al. 2004; Canavier and Landry 2006) however, the L-type channels (Takada et al. 2001) and the SK channels (Yang and Callaway 2006) are known to be distributed throughout the neuron, and dendritic Ca^{2+} oscillations have been documented experimentally (Wilson and Callaway 2000; Chan et al. 2007). This suggests that distribution of the oscillatory mechanism could play a role in defining firing properties of the neuron. The unusual reliance of the pacemaking mechanism in the SNc on calcium influx and accumulation has been connected to the vulnerability of these neurons to stressors leading to Parkinson disease (Chan et al. 2007). However, the relevance of the SOP and the role of Ca^{2+} oscillation has recently been challenged (Guzman et al 2009; Putzier et al 2009b) suggesting that the role attributed to the Ca^{2+} oscillation may need to be revised.

In the case of DA neurons *in vitro*, in contrast to other types of neurons, simply applying a depolarizing current to the soma does not elicit repetitive bursts or even increase the firing rate to levels observed during burst firing *in vivo*. As the level of injected current is increased, a maximum steady firing rate of about 10 Hz is observed. Further increases result in the loss of spiking (Richards et al. 1997), apparently due to inactivation of the spike-generating sodium current leading to depolarization block. The SK current is partially responsible for limiting the maximum observable frequency. Blocking this current only increases the maximum steady frequency to about 20 Hz, and the maximum transient frequency to 30 Hz (Shepard and Bunney 1991), which is still lower than rates observed during bursts *in vivo*, and lower than in many other types of neurons. In this study we sought to identify additional mechanisms of frequency limitation using a computational approach based on a DA model neuron.

Previous DA neuron models distributed either the pacemaking currents (Wilson and Callaway 2000) or the spiking currents (Komendantov et al 2004; Canavier and Landry 2006) throughout the soma and dendrites, but in the present model both types of currents were distributed throughout the soma and dendrites resulting in a coupled

oscillator model within a single neuron (see also Medvedev and Kopell 2001; Medvedev et al. 2003, and Kuznetsov et al. 2006). An important constraint that was imposed on the model in this study, but not on previous models, was to reproduce the frequency limitation in response to the application of a depolarizing current to the soma, both under control conditions and in the presence of SK blockers. Using this model we focus on the control of the firing rate due to the purely intrinsic mechanisms hypothesized to be responsible for limiting the low basal firing rate, rather than on the synaptic mechanisms that are likely to contribute to high frequency firing.

2 Methods

2.1 Model description

The model used in this study is based on an existing DA neuron model (Komendantov et al 2004). The major modifications were that the pacemaking mechanism comprised of the L-type Ca^{2+} and the SK K^{+} currents that was previously located only in the soma was distributed throughout the soma and dendrites, and the model was calibrated to fit a wider range of experimental data, among which was the aforementioned limitation of the frequency in response to an applied depolarizing current pulse. We changed the description of the calcium pump to a non-electrogenic one (Thomas 2009) because the presence of a persistent inward calcium current (Kang and Kitai 1993b) contradicts the assumption of an equal efflux of charge via the calcium pump at equilibrium. We also removed Ca^{2+} mediated inactivation of the L-type calcium current because the steady Ca^{2+} concentration has been shown not to decline during a voltage clamp step over a course of more than 10 s (Wilson and Callaway 2000).

All channels and pumps were assumed to be uniformly distributed in the absence of evidence to the contrary. To our knowledge only the A-type current has been shown to be inhomogeneously distributed. Its maximal conductance in the proximal dendrites was half that at the soma, and the dendritic inactivation curve was shifted by 5 mV in a hyperpolarized direction, in agreement with experimental data (Gentet and Williams 2007) from somatic nucleated patches or outside-out patches excised from the soma or dendrites. Since the voltage dependence and kinetics of the A-type current recorded at the soma vary between different studies (Silva et al. 1990; Liss et al. 2001; Kullmann et al. 2004; Koyama and Appel 2006; Gentet and Williams 2007; Segev and Korngreen 2007), we fixed the ratio of the maximal conductances and the shift of the inactivation function for the dendritic and somatic A-type current in our model, and adjusted the absolute values of the parameters

associated with this current within the experimentally observed ranges to best reproduce the known effects of blocking and augmenting this current.

The symmetric schematic model shown in Fig. 1(a), adapted from Komendantov et al. 2004, had thirteen compartments, including one somatic, four proximal dendritic, and eight distal dendritic compartments. As in previous implementations, only one compartment in each category was integrated due to the assumed symmetry, and the coupling currents were scaled appropriately resulting effectively in a three-compartment model as shown in Fig. 1(b).

In order to verify that the schematic model captured salient features of the dendritic architecture of a real DA neuron, the model parameters established for this model were applied to a multi-compartmental model that was based on the reconstructed morphology of an actual SNc DA neuron (see Fig. 1(c)). It consisted of a total of 41 compartments, including three somatic, four proximal dendritic and thirty-four distal dendritic compartments. A NEURON (Hines and Carnevale 1997) rendering of this multi-compartmental model is shown in Fig. 1(d). The morphology description (Vetter et al. 2001) was obtained from the file labeled Nigra2a955-1 at NeuroMorpho.Org (Ascoli 2006). It consists of 3 somatic and 38 dendritic compartments. The distinction between proximal and distal dendrites is described in the NEURON file dopaminergic.

hoc. Here proximal dendrites comprised the compartments 3–5, 12, 17, 26 and 31–33 and distal dendrites the compartments 1, 2, 6–11, 13–16, 18–25, 27–30 and 34–37. This and other NEURON files used here will be available at <http://senselab.med.yale.edu/modeldb>.

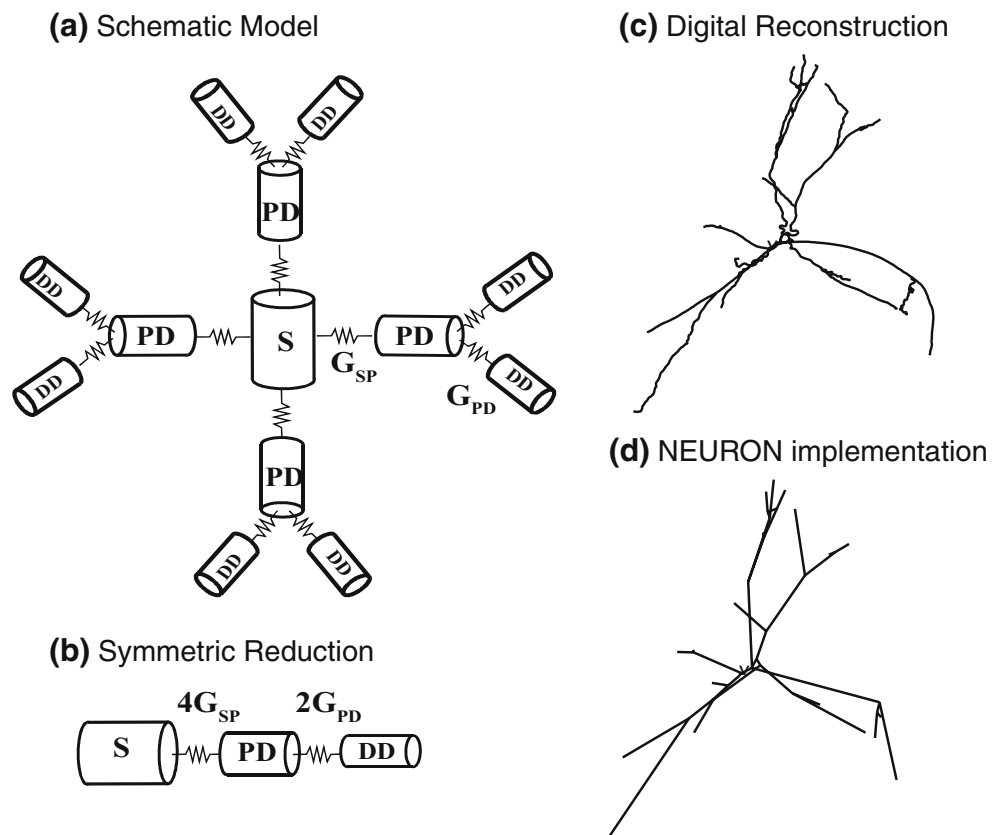
Computer simulations using the schematic model were performed using code written in C, whereas the multi-compartmental model based on the morphological reconstruction was implemented in NEURON. The NEURON parameter *nseg* determines the spatial grid resolution in each compartment. Setting *nseg*=1 for each of the 41 compartments produced results that were indistinguishable from those obtained by automatically adjusting the spatial grid for a conservative parameter setting of *d_lambda*=0.1 and a length constant computed at 100 Hz (for details see Hines and Carnevale 2001). A complete list of equations and model parameters is given in the APPENDIX.

3 Results

3.1 Spontaneous frequency and its modulation by simulated pharmacological treatments

As mentioned in the METHODS section, model parameters of the schematic DA neuron model (Fig. 1(a)) were

Fig. 1 DA neuron model. (a) Symmetric schematic DA neuron model used in this study consisting of one soma, four proximal and eight distal dendritic compartments. (b) Symmetry considerations reduce the 13 compartment model to an effective three compartment. (c) DA neuron reconstructed morphology (Vetter et al. 2001). (d) Multi-compartmental real morphological model as rendered by NEURON



calibrated to reproduce several features of dopaminergic neurons under different pharmacological manipulations. The left panels of Fig. 2 show results of simulations performed using the schematic DA model and the right panels those obtained from the multi-compartmental model with realistic morphology (Fig. 1(d)). All model results are robust whether a stylized schematic model or a model based on a digital reconstruction of a dopaminergic neuron is utilized, indicating that the schematic DA model captured the salient features of the effects of the dendrites on the electrophysiology of dopamine neurons without incorporating the fine details of the dendritic tree. Therefore we use the schematic model to probe the underlying mechanisms. Modeling studies in other neurons have also demonstrated results that are robust to variability in morphology within certain constraints (Komendantov and Ascoli 2009).

Both models reproduce the slow spontaneous firing rate under control conditions (Fig. 2a1 and a2) at about 2 Hz,

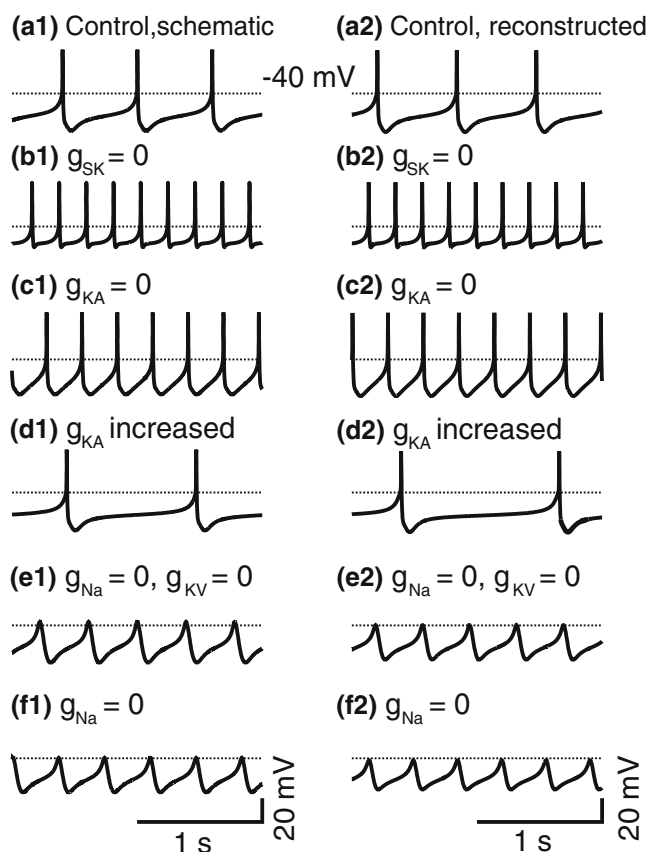


Fig. 2 Simulated responses to pharmacological treatments. Simulated response of DA neurons to various pharmacological manipulations using models with either a schematic (*left column*) or a reconstructed realistic morphology (*right column*). (a) Control; (b) Simulated SK current block; (c) Simulated A-type current block; (d) Simulated potentiation of the A-type current that mimics haloperidol treatment or virtual conductance injection; (e) Simulated blockade of the sodium and the delayed rectifier currents; (f) Simulated blockade of the sodium current only

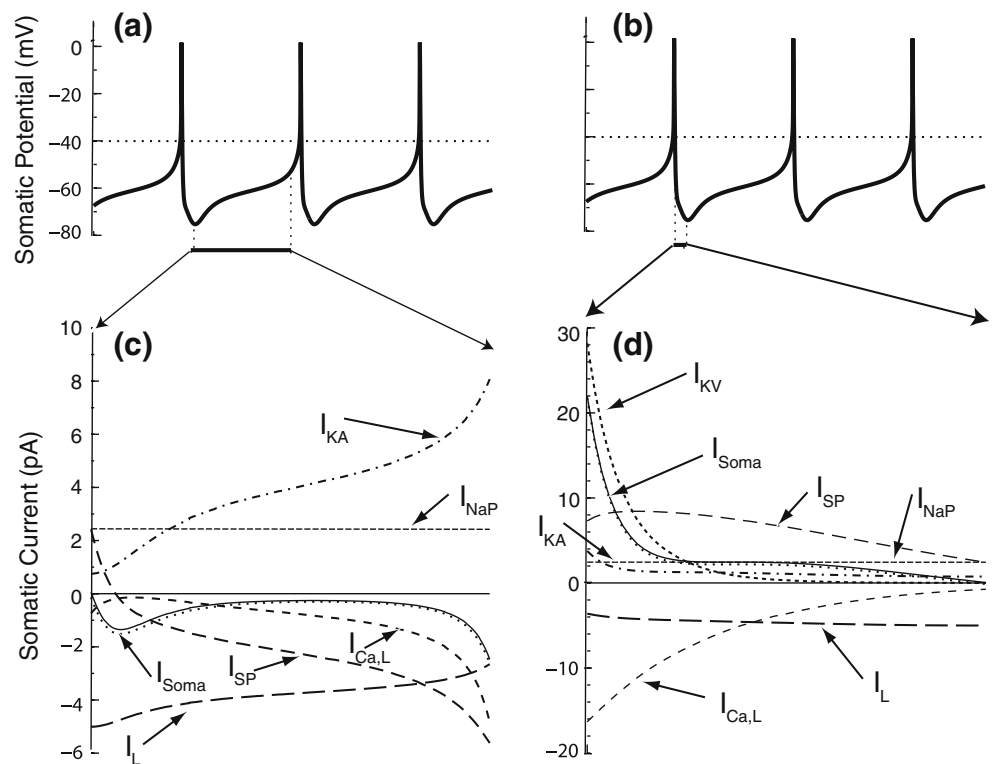
which is in the range of 1.4 to 5.8 Hz reported by Ping and Shepard 1996. Also, in accordance with experimental data (Wolfart et al. 2001), simulated block of the SK current (Fig. 2b1 and b2) increased the firing frequency. The simulated block of the A-current doubled the steady frequency (Fig. 2c1 and c2), consistent with experiments showing that the A-type potassium current blocker heteropodatoxin-3 HpTx3 causes more than a two-fold increase in pacemaking frequency (Liss et al. 2001; Hahn et al. 2003; 2006). An overall 28% increase in the conductance of this current (e.g. in the soma this amounts approximately to a change from 570 to 730 $\mu\text{A}/\text{cm}^2$) decreased the spontaneous frequency (Fig. 2d1 and d2), consistent with the observed effects of the potentiation of the A-type current by haloperidol treatments (Hahn et al. 2003) or of the injection of a virtual A-type current using the dynamic clamp (Hahn et al. 2006; Putzier et al. 2009a). In the schematic DA model, the A-type current has a “window” in the subthreshold membrane potential regime in which there is a steady component that is activated and not inactivated. The A current affects the spontaneous frequency mainly via this hyperpolarizing current that is active during the interspike interval. Finally the simulated blockade of the fast sodium and delayed rectifier currents, respectively, blocked spiking and revealed subthreshold oscillatory potentials (SOP) (Fig. 2e1 and e2) at a steady frequency similar to that observed for spontaneous spiking, consistent with experimental observations (Ping and Shepard 1996). Similarly, simulated block of the fast sodium current only resulted in subthreshold oscillations with a smaller amplitude (Fig. 2f1 and f2), also consistent with experimental observations (Nedergaard et al. 1993; Yung et al. 1991).

As observed in Fig. 2 the schematic model reproduces the responses of DA neurons to these pharmacological manipulations and these results appear indistinguishable from those obtained from a model with a more realistic dendritic architecture. Therefore, in the remainder of this paper all results presented correspond to simulations obtained using the easier to analyze schematic DA model (Fig. 1(a)), which will now be referred to simply as the DA neuron model.

3.2 Membrane currents during spontaneous spiking of DA neurons

Figure 3 shows an analysis of the total somatic current during the inter-spike interval (ISI) of the spontaneously spiking DA neuron model. Panel C shows the contributions from different membrane currents between two spikes, i.e. from the trough of the membrane potential after the first spike to a value around -50 mV prior to the initiation of the next spike as shown in panel A. The main contributions to the total somatic current (I_{Soma} , solid black line) arise from

Fig. 3 Currents contributing to AHP and ISI duration. (a) and (b) show the somatic membrane potential during spontaneous spiking activity, simulated from schematic DA neuron model. Also indicated is the portion of the interspike interval (ISI) analyzed below. (c) and (d) show most important currents that contribute to the total somatic current acting during the time intervals of the ISI indicated in panels A and B. Labeling: I_{KA} , hyperpolarization activated K^+ current; I_{NaP} , electrogenic Na^+ pump; $I_{Ca,L}$, Ca^{2+} L-type channel current, I_{SP} dendritic current; I_L , leak current; I_{Soma} , net contribution from I_{KA} , I_{NaP} , $I_{Ca,L}$, I_{SP} and I_L to total somatic current is indicated by solid curve. In this and subsequent figures, the total somatic current was obtained by multiplying the somatic current densities in the model by the somatic surface area



the leak (I_L), the nearly constant electrogenic sodium pump current (I_{NaP}), the A-type potassium current (I_{KA}), the L-type Ca^{2+} current ($I_{Ca,L}$) and the electrotonic flow of current from the dendrites (I_{SP}). Note that I_{SP} is inward during most of the ISI, which indicates that the contribution of the dendritic SK current during most of the ISI is negligible; instead the dendrites have a depolarizing effect on the soma in the model because of the lower channel density of A-type current in the dendrites compared to the soma. The total contribution from the five currents shown (dotted line) is practically indistinguishable from the total somatic current (solid line), demonstrating that the flow of current through other channels, e.g. somatic SK current, is negligible. The resultant net current is of the order of 0.5 pA during much of the ISI, in agreement with experimental observations (Fig. 2(b) in Khaliq and Bean 2008). Increasing or decreasing the A-current directly decreases or increases the frequency because it is one of the largest currents active during the ISI in spontaneous firing under control conditions. For example, blocking this conductance (Fig. 2c1 and c2) increases the rate of depolarization which shortens the ISI, whereas increasing this conductance (Fig. 2d1 and d2), decreases the rate of depolarization which lengthens the ISI. When a depolarizing current is applied (see below) the A-type current inactivates, reducing its effect in determining the frequency response.

In contrast, blocking the SK current (Fig. 2b1 and b2) increases the frequency dramatically via an indirect mechanism. The mechanism is indirect because, in agree-

ment with Fig. 4(a) of Ping and Shepard 1996, the SK current is not active during most of the ISI, but only immediately after an action potential. Figure 3(d) shows the active currents during the hyperpolarizing phase of the after-hyperpolarization (AHP) shown in panel B. The solid curve gives the total somatic current as before, but the dotted curve now includes a contribution from a sixth current, I_{KV} , the delayed rectifier. In contrast to panel C, I_{SP} is outward during the AHP because the dendritic SK current dominates during this phase. The AHP has an early outward contribution from I_{KV} . There is only a negligible contribution to the total current from the somatic SK channels.

Figure 4 reveals the indirect mechanism of blocking the SK current in the model in terms of the contributions of the membrane currents during the ISI of spontaneously spiking DA neurons. When the SK current is blocked, the AHP is dramatically reduced. Only the early component of the AHP due to I_{KV} remains. Consequently, the L-type calcium current never drops below 2 pA. In contrast, under control conditions, the L-type calcium current is deactivated very effectively in the model by the AHP that result from activation of the dendritic SK current, causing the net current in the model to be less than a picoamp for a large fraction of the interspike interval. The L-type calcium current remains active when the SK channel conductance is set to zero resulting in a faster frequency (Fig. 2b1 and b2) compared to control. The effect of SK blockage might be overstated in the model since it relies on the L-type calcium channel alone as the pacemaking current, whereas other

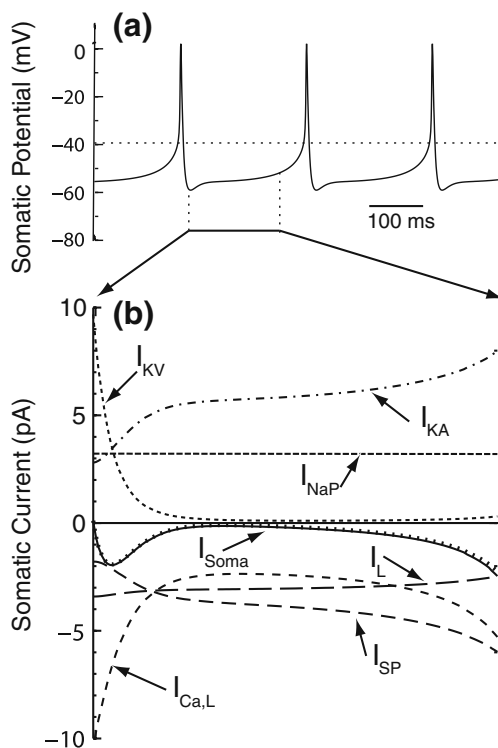


Fig. 4 Currents contributing to ISI duration in the presence of SK channel blocker. **(a)** Somatic membrane potential during spontaneous spiking activity in the presence of SK current blocker, simulated from schematic DA neuron model. Also indicated is the portion of the interspike interval (ISI) analyzed below. **(b)** Currents contributing to the total somatic current during the ISI indicated in panels A. Current labeling is the same as in Fig. 3

calcium and possibly sodium currents likely contribute. Bursting responses and an increase in irregularity have also been reported (Shepard and Bunney 1991; Ping and Shepard 1996) in response to the application of apamin, but these phenomena are not addressed here.

3.3 Maximum frequency and its modulation by SK block

Figure 5 compares the transient and sustained responses of the schematic model (gray symbols) to simulated application of a square pulse of increasing levels of depolarizing current with the experimental data (indicated by black symbols) recorded from dopamine neurons *in vitro* under control conditions (Richards et al. 1997, circles) and in the presence of 1 μ M apamin (Shepard and Bunney 1991, squares). Apamin blocks the SK channel and its effects were simulated by setting g_{SK} to zero. The pulses in these experiments were of 500 ms duration, for the control condition and 800 ms in the simulated SK block condition. Results from simulations correspond to the actual steady-state frequency which is within 0.5 Hz of the values observed at 500 and 800 ms after current pulse onset. Panel A shows the steady, sustained firing rate for the control case

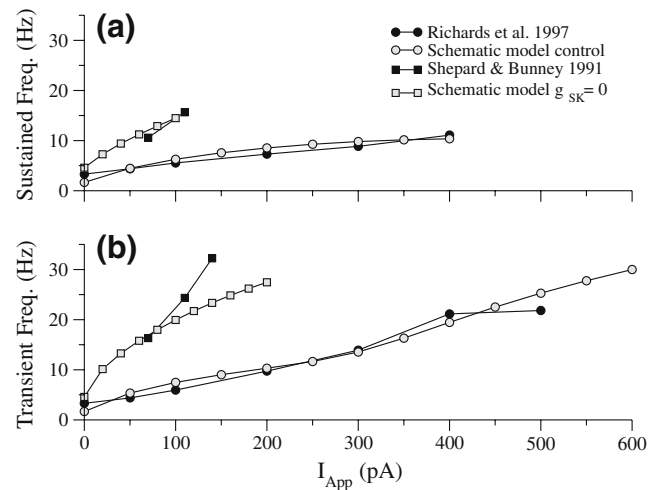


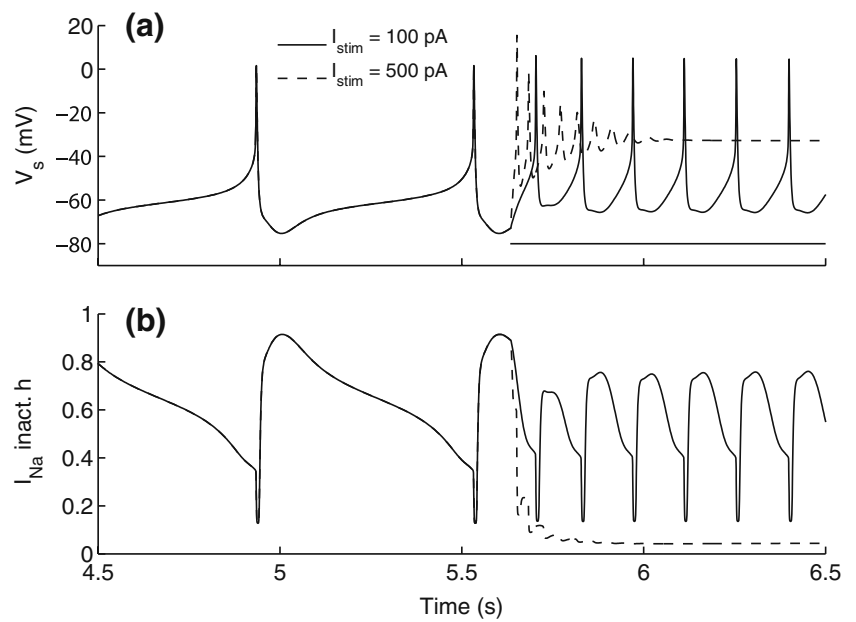
Fig. 5 Frequency versus current plots. Comparison of **(a)** sustained and **(b)** transient frequency responses obtained from schematic DA neuron model under simulated current injection with corresponding experimental data from DA neurons *in vitro*, in the absence (*circles*) and presence (*squares*) of SK blocker apamin. Experimental data from Richards et al. 1997 and Shepard and Bunney 1991 are shown in black and simulated responses in gray

which peaks at about 10 Hz for the DA neuron model and is in good agreement with the 10 Hz observed in the experimental data. In both the model and the data from the literature, blocking the SK current increased the maximum observed frequency to about 15 Hz (Shepard and Bunney 1991, but see also Wolfart et al 2002). For the control case, no results are plotted above a stimulus current of 400 pA because both the real neuron and the DA neuron model enter a state of depolarization block in this range. The most striking effect of SK block in the model was that spiking could no longer be sustained for injected currents in excess of 100 pA, in contrast to the control case in which this limit was greater than 400 pA.

In Fig. 5(b) a comparison is made between the transient responses obtained from the DA neuron model and the corresponding experimental measurements. The maximum transient frequency (the inverse of the ISI) was always observed for the first pair of spikes after stimulus onset, which under control conditions did not exceed about 22 Hz for the experimental data, but reaches somewhat higher values (up to 30 Hz) for the DA neuron model. On the other hand, the transient response of the model (27 Hz) was slightly slower than indicated by the data under SK block (35 Hz). The experimental data shown in Fig. 5 exhibits more frequency adaptation than the model in the presence of SK block, possibly indicating the contribution of an unmodeled process. The response of the model based on the digital reconstruction was very similar to that of the schematic model (not shown) for all cases shown in Fig. 5.

Figure 6 illustrates how the model neuron enters depolarization block. Panel A shows two somatic mem-

Fig. 6 Depolarization block as applied current is increased. **(a)** Somatic membrane potential trace from schematic DA neuron model in response to two values of the simulated applied current: 100 pA (solid line) and 500 pA (dashed line). In the latter case a cessation of the spiking response is observed. Solid thick line indicates that applied current is on. **(b)** Inactivation variable (h) of fast Na^+ current as a function of time for the two cases considered in A. At the larger value of applied current the inactivation of Na^+ current is not removed leading to depolarization block



brane voltage traces, simulated using the DA neuron model for two values of injected current: 100 pA (solid line) and 500 pA (dashed line). In the latter case the neuron enters a state of depolarization block as not enough Na^+ current inactivation can be removed in subsequent cycles after the stimulus current is turned on (indicated by the thick black line). Panel B shows the inactivation level of the Na^+ current plotted as a function of time for the two stimulus currents. Note that during spontaneous activity (first two spikes prior to stimulus

onset) inactivation is almost fully removed after each spike (h approx. 0.9). However, when the current is turned on the DA neuron becomes more depolarized during the interspike interval (ISI) reducing the ability of the AHP to effectively remove inactivation. For a depolarizing current of 500 pA the removal of inactivation by the induced spikes is very weak leading to a state of depolarization block.

Figure 7 shows why DA neurons enter into depolarization block at lower applied currents when the SK channels

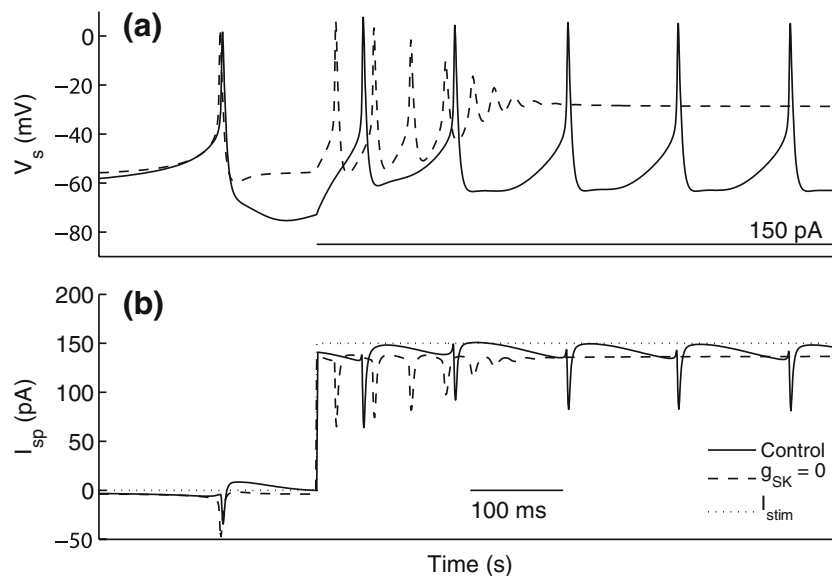


Fig. 7 Depolarization block in the presence and absence of SK current. **(a)** Somatic membrane potential trace from schematic DA neuron model in response to a simulated applied current of 150 pA in the absence (solid line) and presence (dashed line) of SK current blocker. DA neuron enters depolarization block when $g_{SK}=0$. Solid

thick line indicates that applied current is on. **(b)** Dendritic current corresponding to the cases shown in panel A. When the SK channels are blocked this current does not offset the injected current as it occurs in control conditions. The applied current (I_{stim}) is also shown (dotted line) for comparison with the dendritic current

are blocked. Specifically, Fig. 7 shows that the dendritic SK current, manifested at the soma as a component of I_{SP} , tends to offset the depolarizing effect of the applied current. This is illustrated here for the response to a square pulse of 150 pA under control conditions (solid line) and under simulated SK block (dashed line). Panel A shows the membrane voltage traces that have been aligned at the onset of the injected current (thick solid line). Panel B shows the dendritic current (I_{SP}) as a function of time that correspond to the traces in panel A. In the control case (solid line) the evoked dendritic current offsets the applied current (I_{stim} , dotted line) during the ISI, particularly after each spike. These two currents have an opposite sign convention in the model, so if they are equal they cancel each other out. However, when the SK current is blocked ($g_{SK}=0$), dendritic current flowing to the soma decreases (dashed line) causing an increase in the level of depolarization, which makes the removal of Na^+ current inactivation less effective. The difference between the solid and dashed lines reflects the contribution of dendritic SK. The more effective AHP and consequent removal of inactivation of the sodium current when the SK current is present explains why depolarization block occurs only for applied currents greater than 400 pA under control conditions in Fig. 5(a) and for much smaller applied currents (above 100 pA) when the SK current is blocked. The contribution of the dendritic SK current via I_{SP} during the interspike interval in the presence of applied current is in contrast to the lack of contribution of this current during the ISI during spontaneous firing with no applied current (Fig. 3). Although there is also an increase in the somatic SK current, it is approximately 10 times smaller than the corresponding I_{sp} (not shown), and thus has a smaller effect on the spontaneous firing. Moreover the somatic SK current increases gradually as the somatic Ca^{2+} concentration increases while the effect of dendritic SK is almost instantaneous with the onset of the applied current. Other subthreshold currents can also affect the firing frequency and entry point into depolarization block. For example, increasing the conductance of the L-type Ca^{2+} current decreases the minimum current ($I_{app,min}$) required to induce depolarization block. Moreover, we have found that delayed deactivation of the current narrows the spiking range very effectively in agreement with experimental evidence supporting slow deactivation of the L-type Ca^{2+} current in these neurons (Ping and Shepard 1999). This current is modeled with a time constant of up to 18 ms in the subthreshold voltage range, which declines to 0.3 ms at more depolarized potentials. As a result, the Ca^{2+} current peaks immediately after a spike, and effectively opposes the ability of the AHP complex to remove inactivation of the sodium current. If the time constant of activation (and therefore deactivation) is increased, the minimum applied

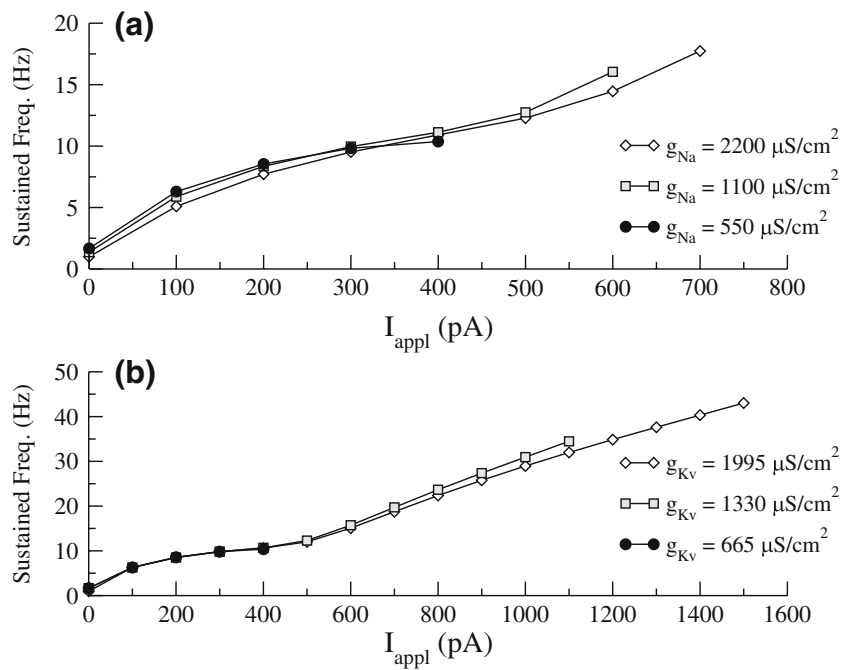
current required to induce depolarization block ($I_{app,min}$) decreases. Therefore, the L-type Ca^{2+} current strongly affects the spiking range in the model. On the other hand, the A-type K^+ current in the model has a negligible effect on the range of depolarizing currents that support spiking and therefore a negligible effect on the maximum observed frequency (not shown). This is because depolarization inactivates this current, nullifying its effect on the firing rate.

3.4 Control of the maximum frequency by the spiking currents

The control of the maximum firing rate by the conductance densities of the principal currents responsible for spiking is illustrated in Fig. 8. Panel A shows that as the value of the Na^+ conductance is doubled from its control value of 550 $\mu S/cm^2$ (black circles) to 1100 $\mu S/cm^2$ (gray squares), little change is observed in the spontaneous firing rate or in the firing rate at any level of depolarizing current injection that previously supported spiking. On the other hand, at an applied current of 500 pA that previously led to depolarization block, spiking is now supported at a higher maximum frequency than before. This trend continues when Na^+ conductance is doubled again to 2200 $\mu S/cm^2$ (white diamonds). Thus, in this parameter range, the only effect of increasing the sodium current density is to rescue the model from depolarization block at the most depolarized values of current injection and thereby to increase the maximum frequency achieved before entering depolarization block. Increasing sodium conductance in this regime does not affect spike frequency at a given level of current, but rather only affects whether spiking can be sustained or not. The minimum sodium conductance that enables spontaneous repetitive spiking as opposed to just the SOP is about 200 $\mu S/cm^2$. The ratio between the actual conductance used in the model and this minimum conductance is 2.75 and is defined as the safety factor in this context. We hypothesize that the safety factor is low in dopamine neurons compared to other types of neurons that can be made to fire repetitively at faster rates.

Depolarization block results when insufficient sodium channel inactivation is removed after one spike to allow the initiation of the next spike, and the level of inactivation increases with increasing depolarization (see Fig. 6). Any manipulation that increases the residual sodium current after an action potential should have the same effect illustrated in Fig. 8(a), that is, to allow spiking at more depolarized levels, and therefore to increase the maximum observable spiking rate. Figure 8(b) illustrates that this is indeed the case. Doubling the delayed rectifier conductance from its control value of 665 $\mu S/cm^2$ (black circles) to 1330 $\mu S/cm^2$ (gray squares) results in only minor changes to the frequency/current curve below the threshold for

Fig. 8 Spiking current conductance densities control the maximum frequency in the schematic model. **(a)** Frequency current plots at different levels of sodium conductance density (g_{Na}). **(b)** Frequency current plots at different levels of the delayed rectifier conductance density (g_{Kv}). All other parameters are as given in the Appendix



depolarization block at the lower conductance value. Above the threshold, this manipulation effectively extends the spiking range (the range of applied currents where repetitive spiking persists) because a deeper and longer after-hyperpolarization removes more inactivation of the sodium current, thereby again increasing the maximum observable firing frequency. Tripling the conductance (white diamonds) continues this trend. Increasing the time constant for the deactivation of the delayed rectifier has a similar effect (not shown) because it also promotes recovery of the sodium current from inactivation after a spike.

A characteristic feature of the sodium spikes produced by DA neurons is their large half-width duration greater than 2 ms (Blythe et al. 2007). The duration of the spike obtained in our simulations is approximately 3 ms. The weak spike-producing currents required to restrict the spiking range in the model also resulted in very wide spikes. The low safety factor for spike generation may be responsible for both distinctive attributes: the low maximum frequency and the wide spikes. The model produces an action potential under control conditions with an amplitude of about 75 mV, similar to that reported by Richards et al. 1997, the study that was used to calibrate the entry of the model into depolarization block.

3.5 Maximum transient frequency depends on the phase of the pacemaker at pulse onset

In experiments, the maximum transient frequency observed during a pulse of applied current was 32 Hz under apamin (Shepard and Bunney 1991) and 22 Hz in control (Richards

et al. 1997). Figure 5 shows that our simulations can reproduce these observed transient frequencies. However, Fig. 9 shows that there is considerable variability in the maximum transient frequency depending upon exactly where in the cycle the depolarizing current pulse is turned on. Panel A shows the somatic membrane potential trace during spontaneous activity and panel B shows the Ca^{2+} oscillation occurring in the soma (solid line), proximal dendrites (dashed line) and distal dendrites (dot-dashed line). Time zero corresponds to the peak of the last spike prior to the onset of the stimulus current. Panel C shows the initial instantaneous firing rate under control conditions (plus signs) as a function of the onset of a 300 pA current pulse relative to the time of the last spike, showing the dependence on the phase of the Ca^{2+} oscillation. Under control conditions (plus sign) higher transient frequencies near 25 Hz are observed when the pulse is initiated near the minimum of the Ca^{2+} oscillation (300 ms) compared to about 10 Hz observed near the maximum which occurs 10 ms after the spike peak. The lower the calcium concentration in the distal dendrites at the time of pulse onset, the faster the transient frequency because the contribution from distal dendritic SK requires some elapsed time to reach its steady value in the presence of applied current (see Fig. 7(b)).

In the control parameter set, the fraction of free Ca^{2+} (f_{Ca}) was set to 0.05 for all compartments. Ca^{2+} buffering is not modeled explicitly, but increasing the buffer concentration would slow the rate of change of free Ca^{2+} in the cytosol and can be approximated in the model by decreasing f_{Ca} . By selective adjusting f_{Ca} in some or all compartments, we can prove that the distal dendrites dominate the determination of the transient frequency. As shown in Fig. 9(c), decreasing f_{Ca}

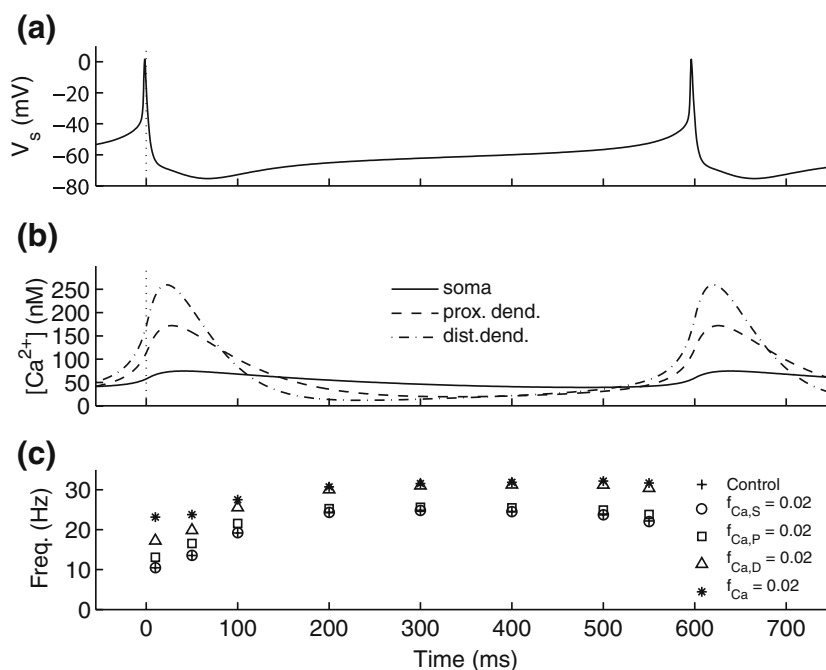


Fig. 9 Dependence of the transient frequency on the phase of dendritic Ca^{2+} oscillation at pulse onset. **(a)** Somatic membrane potential trace from schematic DA neuron model corresponding to spontaneous activity in control conditions. Time scale has been shifted to coincide with time of action potential (*vertical dotted line*) prior to the onset of stimulus current. **(b)** Ca^{2+} oscillation in the soma (*solid*), proximal dendrites (*dash*) and distal dendrites (*dash dot*) occurring simultaneously with voltage trace shown in A. **(c)** Transient frequency response computed from first spike pair, evoked by simulated

injection of a 300 pA stimulus current which is turned on at different times after the occurrence of action potential at 0 s. Results corresponding to control conditions are indicated by a plus sign; open symbols correspond to the transient frequency response obtained when the fraction of free Ca^{2+} (f_{Ca}) decreases from its control value of 0.05 to 0.02 in either soma (*circle*), proximal dendrites (*square*) or distal dendrites (*triangle*); results indicated with an asterisk correspond to the case when the decrease in free Ca^{2+} occurs in all compartments simultaneously

in the distal dendrites alone ($f_{Ca,D}=0.02$) which is indicated by open triangles, has almost the same effect as changing it everywhere ($f_{Ca}=0.02$) indicated by the asterisks. The only exception is that the first two measurements after the spike peak show some contribution from calcium accumulation in the soma and proximal dendrites. Similarly, decreasing f_{Ca} in the soma (open circles) or proximal dendrites (open squares) alone only differs from control (plus signs) for the first two or three points after the spike peak.

3.6 Sustained spiking frequency is not paced by the slow oscillatory potential (SOP)

Figure 10 plots the sustained spiking frequency under control conditions versus the SOP frequency observed after setting g_{Na} to zero for various levels of injected current and for different Ca^{2+} buffering conditions. The idea was to use variations in these two critical parameters to simulate the variability in electrophysiological and biophysical properties that would normally be encountered in a population of dopamine neurons. This was necessary in order to compare model results to experimental data (Guzman et al 2009) from a number of different neurons. As the stimulus current is increased from 0 to 300 pA, the sustained spiking frequency

increases in accordance with the results shown in Fig. 5 (see caption for figure description). There is no apparent correlation between the SOP and spiking frequencies of the DA neuron model clearly showing that the SOP does not pace the steady spiking. The spikes reset the phase of the Ca^{2+} oscillation such that the maximum occurs right after a spike as shown in panels A and B of Fig. 9. These findings are consistent with recent data (Guzman et al. 2009) that showed no correlation between the SOP and spike frequencies across a population of dopamine neurons. Furthermore, a reduction in the fraction of free Ca^{2+} in all model compartments from a value of 0.05 in control (data points indicated with a plus sign) to 0.02, causes a slight increase in the spontaneous firing rate (black circles). This shift in firing rate is consistent with results in Guzman et al. 2009 showing a shortening of the interspike interval after the application of BAPTA (cf. Fig. 3(c) in that publication), after a delay during which the BAPTA presumably diffused into the dendrites.

4 Discussion

The main results of this study can be summarized as follows: (1) the responses of the schematic model shown in

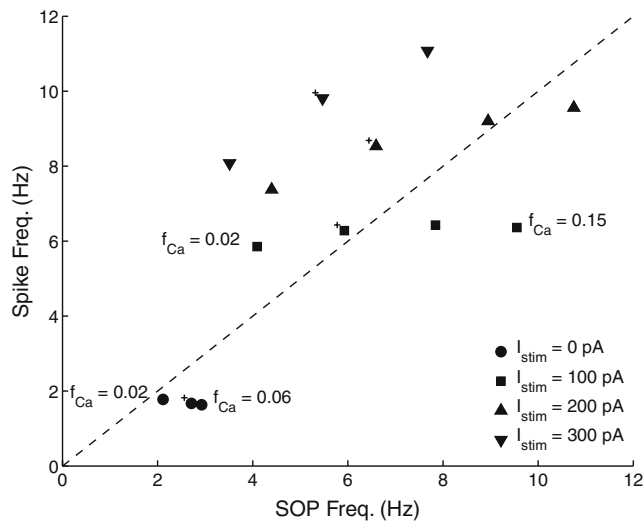


Fig. 10 SOP and spiking frequencies are uncorrelated. Correlation plot between spontaneous spiking and slow oscillatory potential (SOP) frequencies obtained from schematic DA neuron model for different levels of applied current and Ca^{2+} buffering conditions. Moving from left to right, data points indicate increasing values of the fraction of free Ca^{2+} (f_{Ca}): for nonzero applied current these values are 0.02, 0.05, 0.1 and 0.15 and for zero applied current these are 0.02, 0.05 and 0.06. At a constant value of depolarization, indicated by a common symbol, the spiking rate is much flatter than the SOP rate as the rate of change of free Ca^{2+} is increased. This effect is particularly pronounced at $I_{stim}=100$ pA (filled squares). Data points corresponding to control conditions are marked by a plus sign. If the SOP frequency drove the spiking frequency, all points would fall on or near the diagonal

Fig. 1(a) are nearly identical to those of a model based on a digital reconstruction of a DA neuron suggesting that the reduced model captures the salient effects of the dendrites without incorporating all of the details of the dendritic architecture; (2) the dominant somatic currents during the ISI of spontaneous spiking are: the leak, the electrogenic Na^+ pump, the A-type K^+ , the L-type Ca^{2+} and the depolarizing electrotonic contribution from the dendrites due to their lower A current density; furthermore, the somatic SK current is negligible while dendritic SK contributions dominate during the AHP; (3) blocking SK channels increases the spontaneous spiking frequency by decreasing the deinactivation of the L-type current by the AHP, which keeps it more active than in the control case; (4) depolarization block results from a low safety factor for action potential generation; (5) dendritic SK current offsets the depolarizing effects of a current applied to the soma allowing spiking to continue, avoiding depolarization block; (6) the SOP does not pace the sustained spiking frequency; and (7) high frequency transients observed after depolarization applied to the soma depend on the phase of Ca^{2+} oscillations and the rate of Ca^{2+} accumulation, mostly in the distal dendrites.

5 Why DA Neurons cannot achieve fast steady rates in response to somatic depolarization

The hypothesis proposed here is that the safety factor is low in dopamine neurons compared to other types of neurons that can be made to fire repetitively at faster rates, causing inadequate removal of sodium activation at fast rates that leads to depolarization block. The sodium channel density on the soma and dendrites of CA1 pyramidal neurons, for example, is 3000–6000 $\mu S/cm^2$ (Magee and Johnston 1995), similar to what was proposed in earlier models (Komendantov et al. 2004; Canavier and Landry 2006), but much greater than the channel density required to obtain a maximum firing rate in the model that agrees with experimental data (see Fig. 3(a), about 550 $\mu S/cm^2$). The sodium current observed at the soma in the model peaks at 4.5 nA under simulated voltage clamp at -20 mV; the peak sodium current observed experimentally occurs in the same voltage range (-22.0 ± 2.7 mV, Ogata and Tatebayashi 1992), but the peak value observed experimentally is only 1.2–1.5 nA (Ogata and Tatebayashi 1992; Chiodo and Kapatos 1992; Chan et al. 2007), consistent with a sodium current that is even weaker in dopamine neurons than in our model. In addition, L-type Ca^{2+} current in our model effectively opposes the after-hyperpolarizing complex that removes inactivation of sodium channels, contributing to the low safety factor of action potential generation. This proposed hypothesis can be tested by adding a virtual sodium conductance, via the dynamic clamp, to a DA neuron *in vitro*. This addition should leave the spontaneous frequency unaltered but increase the maximum frequencies that can be observed at values of applied depolarizing current that would otherwise produce depolarization block (see Fig. 8). Other explanations for the cessation of firing observed in response to a depolarizing current are possible, such as the recruitment of an adapting current, but less likely since such a current has not been identified despite intensive scrutiny of these cells.

Another possible explanation for the low maximum steady frequencies exhibited in response to depolarization *in vitro* involves the role of slow Ca^{2+} oscillations that is assumed to underlie pacemaking in this cells (Medvedev and Kopell 2001; Medvedev et al. 2003; Wilson and Callaway 2000). Here, the slower frequency of the Ca^{2+} -driven slow oscillatory potentials (SOP) in the soma and proximate dendrites determines the maximum frequencies observed *in vitro*, but can be circumvented *in vivo* if the influence of the SOP in the smaller, faster dendritic compartments is augmented by the activation of distal dendritic NMDA receptors (Kuznetsov et al. 2006). This oscillation was thought to be much more crucial to the maintenance of pacemaking in the substantia nigra par compacta (SNc) compared to the ventral tegmental area

(VTA), and more crucial to the maintenance of pacemaking in the SNc from adult rats compared to juvenile rats (Chan et al. 2007). Nevertheless, this mechanism does not account for the persistence of the frequency limitation when SK channel blockers remove the influence of the oscillation in Ca^{2+} (Shepard and Bunney 1991) on the firing pattern in the SNc. Contrary to the previous role assigned to this oscillation, there is now experimental evidence showing that the frequency of the slow oscillatory potential is not correlated with the spiking frequency during spontaneous activity (Guzman et al. 2009), which agrees with the results in Fig. 10. We hypothesize that the critical features that led to the dissociation of SOP frequency and spiking frequency in both the schematic and more morphologically realistic models include the large ratio of dendritic membrane area to somatic membrane area and the effectively strong coupling between all compartments. These features grant the dendrites a large influence on the DA neuron model dynamics, as is seen in the dominant role of the Ca^{2+} dynamics in the distal dendrites (Fig. 9c) in determining the maximum transient frequencies observed. As is illustrated in Figs. 3, 4, 7 and 9 the role of the dendrites is more complex than that suggested in Wilson and Callaway 2000 and Kuznetsov et al. 2006.

Additional support for the role of a low safety factor is provided by the observation that in the model, the sodium conductance had to be relatively weak to produce a low maximum firing frequency, which further implied that the opposing potassium conductances were relatively weak and slow. This combination led to wider action potentials, thus broad action potentials and low maximum frequencies that can be evoked by depolarization have a common cause in the model. Broad action potentials are characteristic of dopamine neurons, along with other neurons that secrete modulatory transmitters (Bean 2007). The width of an action potential in the dopamine neuron can be 4 ms, compared to 0.180 ms in a cerebellar Purkinje neuron or 0.810 ms in a hippocampal CA1 neuron. Bean 2007 attributed the difference in action potential width to the size and speed of repolarizing potassium currents. A general inverse correlation between firing frequency and action potential width was noted. In this study, we found that the distinctive properties of the DA neuron, namely, low steady and maximum firing frequencies, broad action potentials, and the unusual reliance on subthreshold depolarization by Ca^{2+} channels (which opposes the AHP) are all correlated with a low safety factor for action potential generation.

6 How dopamine neurons produce fast transient firing rates *in vivo*

The issue of whether a separate mechanism is required for burst firing compared to single spike firing is somewhat

controversial. In our models, the observed transient frequencies are sufficient to produce a classically defined burst (Grace and Bunney 1984a, b) with an interspike interval less than 80 ms. These bursts do not require sustained firing, so the limitation of the model to steady pacemaking rates of 10 Hz does not preclude burst firing. The simplest mechanism for bursting is that sufficiently fast transients can be produced simply by depolarization. Blythe et al. 2009, obtained transient rates of 35 Hz in rodent slice preparations by applying depolarizing current pulses to the soma, and argue that no additional mechanism is required for burst production. Frequencies higher than 35 Hz have been observed in unanaesthetized rats (Hyland et al 2002) and monkeys (Schultz 2002) *in vivo*. Simply depolarizing the cell cannot elevate firing rates to this level, which suggests an additional mechanism is required; one possibility is that the voltage dependence of ion channels coupled to synaptic receptors may be crucial in supporting very high transient firing rates. A role for NMDA receptors in eliciting the faster frequencies observed in bursts is supported by the observation that the selective genetic inactivation of NMDA receptors in dopamine neurons (Zweifel et al. 2009) significantly impaired burst firing in freely moving mice. Furthermore, the addition of a virtual NMDA current at the soma is sufficient to induce firing rates observed during burst firing (Deister et al. 2009), so despite an earlier hypothesis that distal dendritic oscillations augmented by activation of distal NMDA receptors were critical for burst production (Kuznetsov et al 2006), a consensus seems to be emerging that changes in the intrinsic frequency of dendritic oscillations are not critical to the production of fast frequencies in dopamine neurons under somatic depolarization.

Our results support this new interpretation and suggest that changes in the basal level of $[\text{Ca}^{2+}]$ in distal dendrites, rather than changes in intrinsic frequency, have a significant effect in the transient frequency response which could contribute to the bursting mechanism. In other words, an afferent excitatory input is predicted to evoke a lower frequency transient if it is received shortly after an action potential than if it is received after the AHP has dissipated (see Fig. 9(c)). This predicted mechanism can only partially account for the elevation in transient firing rates observed during episodes of burst firing *in vivo*. Further studies are required to incorporate the effects of synaptic currents on burst firing. In view of our results on the mechanisms of frequency limitation showing that somatic current stimulation can produce transient firing rates that exceed the 10 Hz limitation for steady rates, but cannot produce rates greater than 35 Hz such as those observed transiently *in vivo* combined with experimental results presented by Zweifel et al. 2009 showing that selective genetic NMDAR inactivation impairs burst firing, it seems likely that burst signaling

to downstream neurons requires the activation of NMDA receptors to enable the DA neuron to respond with sufficiently high transient frequencies.

Acknowledgments This work was supported by National Institutes of Health grants NS 37963 and 61097 to CCC, National Science Foundation grant DMS-0817717 to ASK, and National Institutes of Health grant MH 079276 to CAP. AYK thanks M. Hines and N. Carnevale for advice on NEURON, support from the IUPUI Center for Mathematical Biosciences, Department of Mathematical Sciences at IUPUI, and B. Boukai, C. Wilson for consultation on fitting calcium concentration, and C. Paladini’s and C. Wilson’s labs for help with literature.

Appendix

In the following equations the subscript “i” indicates a nonspecific compartment, whereas the subscripts “d”, “p”, and “s” indicate distal dendritic compartment, proximal dendritic compartment and somatic compartment respectively. All compartments are considered cylindrical in shape with diameter and length given by d_i and L_i , respectively.

Equations governing membrane potential in each compartment:

$$\begin{aligned}
 -C_m(dV_d/dt) &= I_{Na,d} + I_{KA,d} + I_{KV,d} + I_{SK,d} + I_{NaP,d} \\
 &\quad + I_{Ca,L,d} + I_{CaP,d} + I_{L,d} + I_{dp} \\
 -C_m(dV_p/dt) &= I_{Na,p} + I_{KA,p} + I_{KV,p} + I_{SK,p} + I_{NaP,p} \\
 &\quad + I_{Ca,L,p} + I_{CaP,p} + I_{L,p} + I_{pd} + I_{ps} \\
 -C_m(dV_s/dt) &= I_{Na,s} + I_{KA,s} + I_{KV,s} + I_{SK,s} + I_{NaP,s} \\
 &\quad + I_{Ca,L,s} + I_{CaP,s} + I_{L,s} + I_{sp} - I_{stim}
 \end{aligned}$$

Here I_{stim} is the stimulus current applied to the soma.

Linear leakage current:

$$I_{L,i} = I_{L,Na,i} + I_{L,K,i} + I_{L,Ca,i}$$

where

$$\begin{aligned}
 I_{L,K,i} &= g_{L,K,i}(V_i - E_K); I_{L,Na,i} = g_{L,Na,i}(V_i - E_{Na,i}); \\
 I_{L,Ca,i} &= g_{L,Ca,i}(V_i - E_{Ca}); \\
 E_{Na,i} &= (RT/F) \ln([Na]_{out}/[Na]_{in,i})
 \end{aligned}$$

Sodium pump current:

$$I_{NaP,i} = I_{NaP,max,i} / \left(1 + \left(K_{m,Na} / [Na]_{in,i} \right)^{1.5} \right)$$

Sodium balance:

$$\begin{aligned}
 d[Na]_{in,d} / dt &= 4 \times f_d (-I_{Na,d} - I_{L,Na,d} - 3I_{NaP,d}) / (d_d F) \\
 d[Na]_{in,p} / dt &= 4 \times f_p (-I_{Na,p} - I_{L,Na,p} - 3I_{NaP,p}) / (d_p F) \\
 d[Na]_{in,s} / dt &= 4 \times f_s (-I_{Na,s} - I_{L,Na,s} - 3I_{NaP,s}) / (d_s F)
 \end{aligned}$$

Calcium pump current:

$$I_{CaP,i} = I_{CaP,max} [Ca^{2+}]_{in,i} / \left([Ca^{2+}]_{in,i} + K_{m,CaP} \right)$$

Calcium Balance:

$$d[Ca^{2+}]_{in,i} / dt = 2 \times f_{Ca} (I_{Ca,L,i} + I_{CaP,i} + I_{L,Ca,i}) / (d_i F)$$

Fast sodium current:

$$\begin{aligned}
 I_{Na,i} &= g_{Na,i} m^3 h_i (V_i - E_{Na,i}) \\
 dm_i / dt &= [1 / \{1 + \exp[(V_{half,m,i} - V_i) / 6.0]\} - m_i] / \tau_m \\
 dh_i / dt &= (1 / \{1 + \exp[(V_{half,h,i} - V_i) / 7.8]\} - h_i) / \tau_h \\
 \tau_m &= 1.0 / \{1 + \exp[(V_i + 45.0) / 1.5]\} \\
 &\quad - 1.0 / \{1 + \exp[(V_i + 65) / 0.5]\} + 0.04 \\
 \tau_h &= 168.0 / \{1 + \exp[(V_i + 29) / 4.5]\} \\
 &\quad - 168.0 / \{1 + \exp[(V_i + 49) / 2.0]\} + 2.0
 \end{aligned}$$

Calcium current:

$$\begin{aligned}
 I_{Ca,L,i} &= g_{Ca,L} d_{L,i} (V_i - E_{Ca}) \\
 dd_{L,i} / dt &= (1 / \{1 + \exp[-(V_i + 45.0) / 0.5]\} - d_{L,i}) / \tau_{dL} \\
 \tau_{dL} &= \tau_{Ca} \exp[-(V_i + 70.0)^2 / 625] + 0.3
 \end{aligned}$$

Delayed rectifier current:

$$\begin{aligned}
 I_{KV,i} &= g_{KV,i} n^3 i (V_i - E_K) \\
 dn_i / dt &= (1 / \{1 + \exp[-(25.0 - V_i) / 12.0]\} - n_i) / \tau_n \\
 \tau_n &= \tau_{KV} / \{1 + \exp[(V_i + 39.0) / 8.0]\} + 1.0
 \end{aligned}$$

Transient outward potassium current:

$$\begin{aligned}
 I_{KA,i} &= g_{KA,i} p_i^3 q_i (V_i - E_K) \\
 dq_i / dt &= (1 / \{1 + \exp[(V_i + V_{half,q,i}) / S_{q,i}]\} - q_i) / 20.0 \\
 dp_i / dt &= (1 / \{1 + \exp[-(V_i + 43.0) / 24.0]\} - p_i) / \tau_p \\
 \tau_p &= 2.0 \exp[-(V_i + 50.0)^2 / 550.0] + 1.1
 \end{aligned}$$

SK potassium current:

$$I_{SK,i} = g_{SK} / \left[1 + \left(K_{m,SK} / [Ca^{2+}]_{in,i} \right)^4 \right] (V_i - E_K)$$

Intercompartmental coupling currents:

$$\begin{aligned}
 I_{dp} &= g_{dp} (V_d - V_p); I_{pd} = g_{pd} (V_p - V_d); \\
 I_{ps} &= g_{ps} (V_p - V_s); I_{sp} = g_{sp} (V_s - V_p); \\
 g_{sp} &= 4 \times 10^8 G_{sp} / (\pi d_p L_p); g_{ps} = 10^8 G_{sp} / (\pi d_p L_p); \\
 g_{pd} &= 2 \times 10^8 G_{pd} / (\pi d_p L_p); g_{dp} = 10^8 G_{pd} / (\pi d_d L_d); \\
 G_{sp} &= 10^2 \pi d_p^2 d_s^2 / \left[2R_a (L_p d_s^2 + L_s d_p^2) \right] \\
 G_{pd} &= 10^2 \pi d_p^2 d_d^2 / \left[2R_a (L_p d_d^2 + L_d d_p^2) \right]
 \end{aligned}$$

Parameters

The same parameters were used for the models with schematic morphology and reconstructed morphology. The only difference was in the morphology.

$C_m = 1 \mu\text{F}/\text{cm}^2$; $R_a = 40 \Omega \text{cm}$; $R = 8,314 \text{ J/kg mol K}$;
 $F = 96520 \text{ C/mol}$; $T = 308.15 \text{ K}$;
 $d_d = 1.5 \mu\text{m}$; $d_p = 3 \mu\text{m}$; $d_s = 15 \mu\text{m}$; $L_d = 350 \mu\text{m}$;
 $L_p = 150 \mu\text{m}$; $L_s = 25 \mu\text{m}$;
 $E_k = -90 \text{ mV}$; $E_{Ca} = 120 \text{ mV}$;
 $V_{\text{half},m,i} = -34.6 \text{ mV}$; $V_{\text{half},h,i} = -56.8 \text{ mV}$; $V_{\text{half},q,s} = -56 \text{ mV}$;
 $S_{q,s} = 8 \text{ mV}$; $V_{\text{half},q,p} = V_{\text{half},q,d} = -60 \text{ mV}$; $S_{q,p} = S_{q,d} = 5 \text{ mV}$;
 $\tau_{K_v} = 19.0 \text{ ms}$; $\tau_{Ca} = 18.0 \text{ ms}$;
 $[\text{Na}]_{\text{out}} = 145 \text{ mM}$; $K_{M,SK} = 0.00019 \text{ mM}$;
 $K_{M,CaP} = 0.0005 \text{ mM}$; $K_{M,Na} = 10 \text{ mM}$;
 $f_i = 2$; $f_{Ca} = 0.05$;
 $I_{CaP,max,i} = 0.00191 \text{ mA}/\text{cm}^2$; $I_{NaP,max,i} = 0.0092 \text{ mA}/\text{cm}^2$;
 $g_{L,Na,i} = 2.375 \mu\text{S}/\text{cm}^2$; $g_{L,Ca,i} = 0.0136 \mu\text{S}/\text{cm}^2$;
 $g_{L,K,i} = 5.5 \mu\text{S}/\text{cm}^2$;
 $g_{Na,i} = 550 \mu\text{S}/\text{cm}^2$; $g_{K_v,i} = 665 \mu\text{S}/\text{cm}^2$;
 $g_{Ca,L,i} = 11.196 \mu\text{S}/\text{cm}^2$; $g_{SK,i} = 59 \mu\text{S}/\text{cm}^2$;
 $g_{K_A,d} = 266 \mu\text{S}/\text{cm}^2$; $g_{K_A,p} = 285 \mu\text{S}/\text{cm}^2$;
 $g_{K_A,s} = 570 \mu\text{S}/\text{cm}^2$;

References

- Amini, B., Clark, J. W., & Canavier, C. C. (1999). Calcium dynamics underlying pacemaker-like burst firing oscillations in midbrain dopaminergic neurons: A computational study. *Journal of Neurophysiology*, 82, 2249–2261.
- Ascoli, G. A. (2006). Mobilizing the base of neuroscience data: the case of neuronal morphologies. *Nature Reviews Neuroscience*, 7(4), 318–324.
- Bean, B. (2007). The action potential in mammalian central neurons. *Nature Reviews Neuroscience*, 8, 451–465.
- Bernheimer, H., Birkmayer, W., Hornykiewicz, O., Jellinger, K., & Seitelberger, F. (1973). Brain dopamine and the syndromes of Parkinson and Huntington. Clinical, morphological and neurochemical correlations. *Journal of Neurological Science*, 20, 415–455.
- Blythe, S., Wokosin, D., Atherton, J., & Bevan, M. D. (2009). Cellular mechanisms underlying burst firing in substantia nigra dopamine neurons. *Journal of Neuroscience*, 29(49), 15531–15541.
- Blythe, S., Atherton, J., & Bevan, M. (2007). Synaptic activation of dendritic AMPA and NMDA receptors generates transient high-frequency firing in substantia nigra dopamine neurons *in vitro*. *Journal of Neurophysiology*, 97, 2837–2850.
- Canavier, C. C., & Landry, R. S. (2006). An increase in AMPA and a decrease in SK conductance increase burst firing by different mechanisms in a model of a dopamine neuron *in vivo*. *Journal of Neurophysiology*, 96(5), 2549–2563.
- Carlson, N. R. (1999). *Foundations of Physiological Psychology* (4th ed.). Needham Heights, MA: Allyn and Bacon.
- Chan, C. S., Guzman, J. N., Ilijic, E., Mercer, J. N., Rick, C., Tkatch, T., et al. (2007). 'Rejuvenation' protects neurons in mouse models of Parkinson's disease. *Nature*, 447(7148), 1081–1086.
- Chiodo, L., & Kapatos, G. (1992). Membrane properties of identified mesencephalic dopamine neurons in primary dissociated cell culture. *Synapse*, 11, 294–309.
- Deister, C. A., Teagarden, M. A., Wilson, C. J. and Paladini, C. A. (2009). An intrinsic neural oscillator underlies dopaminergic neuron bursting. *Journal of Neuroscience*, in press.
- Gentet, L. J., & Williams, S. R. (2007). Dopamine gates action potential backpropagation in midbrain dopaminergic neurons. *Journal of Neuroscience*, 27(8), 1892–1901.
- Grace, A. A., & Bunney, B. S. (1984a). The control of firing pattern in nigral dopamine neurons: single spike firing. *Journal of Neuroscience*, 4, 2866–2876.
- Grace, A. A., & Bunney, B. S. (1984b). The control of firing pattern in the nigral dopamine neurons: Burst firing. *Journal of Neuroscience*, 4, 2877–2890.
- Guzman, J. N., Sánchez-Padilla, J., Chan, C. S., & Surmeier, D. J. (2009). Robust pacemaking in substantia nigra dopaminergic neurons. *Journal of Neuroscience*, 29(35), 11011–11019.
- Hahn, J., Tse, T. E., & Levitan, E. S. (2003). Long-term K_v channel-mediated dampening of dopamine neuron excitability by the antipsychotic drug haloperidol. *Journal of Neuroscience*, 23(34), 10859–10866.
- Hahn, J., Kullmann, P. H., Horn, J. P., & Levitan, E. S. (2006). D2 autoreceptors chronically enhance dopamine neuron pacemaker activity. *Journal of Neuroscience*, 26(19), 5240–5247.
- Hines, M. L., & Carnevale, N. T. (1997). The NEURON simulation environment. *Neural Computations*, 9(6), 1179–1209.
- Hines, M. L., & Carnevale, N. T. (2001). Neuron: A tool for neuroscientists. *The Neuroscientist*, 7, 123–135.
- Hyland, B. I., Reynolds, J. N. J., Hay, J., Perk, C. G., & Miller, R. (2002). Firing modes of midbrain dopamine cells in the freely moving rat. *Neuroscience*, 114, 475–492.
- Khaliq, Z. M., & Bean, B. P. (2008). Dynamic, Nonlinear Feedback Regulation of Slow Pacemaking by A-Type Potassium Current in Ventral Tegmental Area Neurons. *Journal of Neuroscience*, 28(43), 10905–10917.
- Kang, Y., & Kitai, S. T. (1993a). Calcium spike underlying rhythmic firing in dopaminergic neurons of the rat substantia nigra. *Neuroscience Research*, 18, 195–207.
- Kang, Y., & Kitai, S. T. (1993b). A whole cell patch-clamp study on the pacemaker potential in dopaminergic neurons of the rat substantia nigra compacta. *Neuroscience Research*, 18, 209–221.
- Komendantov, A. O., & Ascoli, G. A. (2009). Dendritic excitability and neuronal morphology as determinants of synaptic efficacy. *Journal of Neurophysiology*, 101(4), 1847–1866.
- Komendantov, A. O., Komendantova, O. G., Johnson, S. W., & Canavier, C. C. (2004). A modeling study suggests complementary roles for GABAA and NMDA receptors and the SK channel in regulating the firing pattern in midbrain dopamine neurons. *Journal of Neurophysiology*, 91, 346–357.
- Koyama, S., & Appel, S. (2006). A-type K^+ current of dopamine and GABA neurons in the ventral tegmental area. *Journal of Neurophysiology*, 96, 544–554.
- Kullmann, P. H., Wheeler, D. W., Beacom, J., & Horn, J. P. (2004). Implementation of a fast 16-Bit dynamic clamp using LabVIEW-RT. *Journal of Neurophysiology*, 91(1), 542–554.
- Kuznetsov, A. S., Kopell, N. J., & Wilson, C. J. (2006). Transient high-frequency firing in a coupled-oscillator model of the mesencephalic dopaminergic neuron. *Journal of Neurophysiology*, 95, 932–937.
- Liss, B., Franz, O., Sewing, S., Bruns, R., Neuhoff, H., & Roeper, J. (2001). Tuning pacemaker frequency of individual dopaminergic neurons by $Kv4.3L$ and $KChip3.1$ transcription. *EMBO Journal*, 20(20), 5715–5724.
- Magee, J. C., & Johnston, D. (1995). Characterization of single voltage-gated Na^+ and Ca^{2+} channels in apical dendrites of rat CA1 pyramidal neurons. *Journal of Physiology*, 487, 67–90.
- Medvedev, G. S., & Kopell, N. (2001). Synchronization and transient dynamics in chains of electrically coupled FitzHugh-Nagumo

- oscillations. *SIAM Journal of Applied Mathematics*, 61, 1763–1801.
- Medvedev, G. S., Wilson, C. J., Callaway, J. C., & Kopell, N. (2003). Dendritic synchrony and transient dynamics in a coupled oscillator model of the dopaminergic neuron. *Journal of Computational Neuroscience*, 15, 53–69.
- Nedergaard, S., Flatman, J. A., & Engberg, I. (1993). Nifedipine-and omega-conotoxin-sensitive Ca^{2+} conductances in guinea-pig substantia nigra pars compacta neurones. *Journal of Physiology (London)*, 466, 727–747.
- Ogata, N., & Tatebayashi, H. (1992). Na^+ -current kinetics are not the determinants of the action potential duration in neurons of the rat ventral tegmental area. *Brain Research Bulletin*, 29, 691–695.
- Ping, H. X., & Shepard, P. D. (1996). Apamin-sensitive Ca^{2+} -activated K^+ channels regulate pacemaker activity in nigral neurons. *NeuroReport*, 7, 809–814.
- Ping, H. X., & Shepard, P. D. (1999). Blockade of SK-type Ca^{2+} -activated K^+ channels uncovers a Ca^{2+} -dependent slow afterdepolarization in nigral dopamine neurons. *Journal of Neurophysiology*, 81, 977–984.
- Putzier, I., Kullmann, P. H. M., Horn, J. P., & Levitan, E. S. (2009a). Dopamine neuron responses depend exponentially on pacemaker interval. *Journal of Neurophysiology*, 101(2), 926–33. Epub 2008 Dec 10.
- Putzier, I., Kullmann, P. H. M., Horn, J. P., & Levitan, E. S. (2009b). $\text{Ca}_v1.3$ channel voltage dependence, not Ca^{2+} selectivity, drives pacemaker activity and amplifies bursts in nigral dopamine neurons. *Journal of Neuroscience*, 29(49), 15414–15419.
- Richards, C. D., Shiroyama, T., & Kitai, S. T. (1997). Electrophysiological and immunocytochemical characteristics of GABA and dopamine neurons in the substantia nigra of the rat. *Neuroscience*, 80, 545–557.
- Schultz, W. (2002). Getting formal with dopamine and reward. *Neuron*, 36, 241–263.
- Segev, D., & Korngreen, A. (2007). Kinetics of two voltage-gated K^+ conductances in substantia nigra dopaminergic neurons. *Brain Research*, 1173, 27–35.
- Shepard, P. D., & Bunney, B. S. (1991). Repetitive firing properties of putative dopamine-containing neurons *in vitro*: regulation by an apamin-sensitive Ca^{2+} -activated K^+ conductance. *Experimental Brain Research*, 86, 141–150.
- Silva, N., Pechura, C., & Barker, J. (1990). Postnatal rat nigrostriatal dopaminergic neurons exhibit five types of potassium conductances. *Journal of Neurophysiology*, 64(1), 262–272.
- Strange, P. G. (2001). Antipsychotic drugs: importance of dopamine receptors for mechanisms of therapeutic actions and side effects. *Pharmacology Review*, 53, 119–133.
- Surmeier, D. J., Mercer, J. N., & Chan, C. S. (2005). Autonomous pacemakers in the basal ganglia: who needs excitatory synapses anyway? *Current Opinion in Neurobiology*, 15, 312–318.
- Takada, M., Kang, Y., & Imanishi, M. (2001). Immunohistochemical localization of voltage-gated calcium channels in substantia nigra dopamine neurons. *European Journal of Neuroscience*, 13, 757–762.
- Thomas, R. C. (2009). The plasma membrane calcium ATPase (PMCA) of neurones is electroneutral and exchanges 2 H^+ for each Ca^{2+} or Ba^{2+} ion extruded. *Journal of Physiology*, 587, 315–327.
- Vetter, P., Roth, A., & Hausser, M. (2001). Propagation of action potentials in dendrites depends on dendritic morphology. *Journal of Neurophysiology*, 85, 926–937.
- Wilson, C. J., & Callaway, J. C. (2000). A coupled oscillator model of the dopaminergic neuron of the substantia nigra. *Journal of Neurophysiology*, 83, 3084–3100.
- Wise, R. A. (2004). Dopamine, learning and motivation. *Nature Review Neuroscience*, 5, 483–494.
- Wolfart, J., Neuhoff, H., Franz, O., & Roeper, J. (2001). Differential expression of the small-conductance, calcium-activated potassium channel SK3 is critical for pacemaker control in dopaminergic midbrain neurons. *Journal of Neuroscience*, 21(10), 3443–3456.
- Wolfart, J., & Roeper, J. (2002). Selective coupling of T-type calcium channels to SK potassium channels prevents intrinsic bursting in dopaminergic midbrain neurons. *Journal of Neuroscience*, 22(9), 3404–3413.
- Yang, X., & Callaway, J. (2006). Dendritic contribution to hyperpolarization recorded at the soma in SNc dopaminergic neurons. *Society of Neuroscience Annual Meeting*, abstract 254.7.
- Yung, W. H., Hausser, M. A., & Jack, J. J. (1991). Electrophysiology of dopaminergic and non-dopaminergic neurones of the guinea-pig substantia nigra pars compacta *in vitro*. *Journal of Physiology*, 436, 643–667.
- Zweifel, L. S., Parker, J. G., Lobb, C. J., Rainwater, A., Wall, V. Z., Fadok, J. P., et al. (2009). Disruption of NMDAR-dependent burst firing by dopamine neurons provides selective assessment of phasic dopamine-dependent behavior. *PNAS*, 106, 7281–7288.